J Physiol 587.13 (2009) pp 3233–3250

The Journal of Physiology

Activation of mGluR5 induces spike afterdepolarization and enhanced excitability in medium spiny neurons of the nucleus accumbens by modulating persistent Na^+ currents

Marcello D'Ascenzo[1], Maria Vittoria Podda[1], Tommaso Fellin[2], Gian Battista Azzena[1], Philip Haydon[3] and Claudio Grassi[1]

[1] *Institute of Human Physiology, Medical School, Catholic University 'S. Cuore', Rome, Italy*
[2] *Italian Institute of Technology, Genoa, Italy*
[3] *Department of Neuroscience, Tufts University, Boston, MA, USA*

The involvement of metabotropic glutamate receptors type 5 (mGluR5) in drug-induced behaviours is well-established but limited information is available on their functional roles in addiction-relevant brain areas like the nucleus accumbens (NAc). This study demonstrates that pharmacological and synaptic activation of mGluR5 increases the spike discharge of medium spiny neurons (MSNs) in the NAc. This effect was associated with the appearance of a slow afterdepolarization (ADP) which, in voltage-clamp experiments, was recorded as a slowly inactivating inward current. Pharmacological studies showed that ADP was elicited by mGluR5 stimulation via G-protein-dependent activation of phospholipase C and elevation of intracellular Ca^{2+} levels. Both ADP and spike aftercurrents were significantly inhibited by the Na^+ channel-blocker, tetrodotoxin (TTX). Moreover, the selective blockade of persistent Na^+ currents (I_{NaP}), achieved by NAc slice pre-incubation with 20 nM TTX or 10 μM riluzole, significantly reduced the ADP amplitude, indicating that this type of Na^+ current is responsible for the mGluR5-dependent ADP. mGluR5 activation also produced significant increases in I_{NaP}, and the pharmacological blockade of this current prevented the mGluR5-induced enhancement of spike discharge. Collectively, these data suggest that mGluR5 activation upregulates I_{NaP} in MSNs of the NAc, thereby inducing an ADP that results in enhanced MSN excitability. Activation of mGluR5 will significantly alter spike firing in MSNs *in vivo*, and this effect could be an important mechanism by which these receptors mediate certain aspects of drug-induced behaviours.

(Received 19 March 2009; accepted after revision 7 May 2009; first published online 11 May 2009)

Corresponding author C. Grassi: Institute of Human Physiology, Medical School, Catholic University 'S. Cuore'; Largo Francesco Vito 1, 00168 Rome, Italy. Email: grassi@rm.unicatt.it

Abbreviations aCSF, artificial cerebrospinal fluid; ADP, afterdepolarization; AP, action potential; CB-DMB, [*N*-(4-chlorobenzyl)]2,4-dimethylbenzamyl; D-AP5, D-(−)-2-amino-5-phosphonopentanoic acid; DHPG, (*RS*)-3,5-dihydroxyphenylglycine; I_{NaP}, persistent Na^+ currents; I_{NaR}, resurgent Na^+ currents; mGluR5, type 5 metabotropic glutamate receptors; MPEP, 2-methyl-6-(phenylethynyl)pyridine hydrochloride; MSNs, medium spiny neurons; NAc, nucleus accumbens; PLC, phospholipase C.

The nucleus accumbens (NAc), part of the ventral striatum in the basal ganglia, plays a critical role in translating emotional, motivational and rewarding stimuli into behaviour (Nestler, 2001; Goto & Grace, 2008). Together with the ventral tegmental area and associated limbic structures, the NAc is the site of the long-lasting, drug-induced neuroadaptations underlying addiction (Kauer & Malenka, 2007). Dopamine is traditionally considered the key neurotransmitter in these processes, but glutamate involvement is also solidly supported by evidence from animal models of addiction (McFarland *et al.* 2003; LaLumiere & Kalivas, 2008). Although many forms of glutamate-dependent neuroplasticity in the NAc are manifested by changes in ionotropic glutamate receptor signalling (Thomas *et al.* 2001; Everitt & Wolf, 2002; Kauer & Malenka, 2007), increasing evidence points to type 5 metabotropic glutamate receptors (mGluR5) as important mediators of effects produced by addictive drugs. These group I mGluRs are coupled to $G_{q/11}$ proteins, and their stimulation triggers phospholipase C (PLC) activation, mobilization of intracellular Ca^{2+}, and ultimately modulation of various

DOI: 10.1113/jphysiol.2009.172593

ion channels (Pin & Duvoisin, 1995). mGluR5-knockout prevents cocaine self-administration in mice (Chiamulera *et al.* 2001) and, in wild-type mice, the mGluR5 antagonist 2-methyl-6-(phenylethynyl)pyridine hydrochloride (MPEP) decreases cocaine, morphine and nicotine self-administration, and drug-seeking behaviour (Popik & Wróbel, 2002; Aoki *et al.* 2004; Tessari *et al.* 2004).

In medium spiny neurons (MSNs), the predominant neuronal type in the NAc, mGluR5 is largely located postsynaptically in dendrites (Mitrano & Smith, 2007). Functional studies of mGluR5 in the NAc have shown that their activation depresses glutamatergic synaptic transmission and mediates a form of cannabinoid-dependent long-term synaptic depression (Robbe *et al.* 2002). We recently demonstrated that activation of mGluR5 located on astrocytes leads to Ca^{2+}-dependent glutamate release from these glial cells, which, in turn, causes a powerful excitation driving trains of action potentials (APs) in MSNs (D'Ascenzo *et al.* 2007). Little is known, however, about the effects of mGluR5 activation on MSN spike firing – a major mechanism by which these cells process information.

In situ, MSNs oscillate between two distinct membrane states (Wilson & Kawaguchi, 1996; Goto & O'Donnell, 2001). The so-called down-state is characterized by relative hyperpolarization (*ca* −85 mV) and the absence of APs, while the up-state is triggered by temporally coherent and convergent excitatory synaptic input bringing membrane potential to values of approximately −55 mV that are much closer to the AP firing threshold. The duration of this state and the AP-discharge rate both seem to be influenced by intrinsic voltage-dependent currents (Galarraga *et al.* 1994; Shen *et al.* 2004).

In this study, we found that activation of postsynaptic mGluR5 in NAc MSNs increases the AP firing rates induced by depolarizing current injection mimicking the up-state. This enhanced excitability is associated with a spike afterdepolarization (ADP) that is mediated primarily by the augmentation of persistent Na^+ currents. Activation of Na^+/Ca^{2+} exchanger also contributes to the mGluR5-mediated enhancement of MSN excitability by eliciting membrane depolarization.

Methods

Ethical approval

All animal procedures were approved by the Ethical Committee of the Catholic University and complied with Italian Ministry of Health guidelines and with national laws (Legislative decree 116/1992) and European Union guidelines on animal research (No. 86/609/EEC).

Slice preparation. Coronal slices (300 μm thick) containing the NAc were prepared from C57BL/6 mice (13–17-days old) with standard procedures (D'Ascenzo *et al.* 2007). Briefly, the animals were anaesthetized with halothane (Sigma, Milan, Italy) and decapitated. The brain was rapidly removed and placed in ice-cold cutting solution containing (in mM): 120 NaCl, 3.2 KCl, 1 KH_2PO_4, 26 $NaHCO_3$, 2 $MgCl_2$, 1 $CaCl_2$, 10 glucose, 2 sodium pyruvate, and 0.6 ascorbic acid (pH 7.4, 95% O_2–5% CO_2). Slices were cut with a vibrating microtome (VT1000S, Leica Microsystems, GmbH, Wetzlar, Germany) and incubated in cutting solution at 34°C for 60 min and then at room temperature until use.

Patch-clamp recordings. Slices were transferred to a submerged recording chamber and continuously perfused with artificial cerebrospinal fluid (aCSF) bubbled with 95% O_2–5% CO_2 (pH 7.4). The aCSF contained (in mM): 120 NaCl, 3.2 KCl, 1 NaH_2PO_4, 1 $MgCl_2$, 2 $CaCl_2$, 26 $NaHCO_3$, 10 glucose. The flow rate was kept at 1.5 ml min^{-1} with a peristaltic pump (Minipuls 3, Gilson, Villiers, France), and bath temperature was maintained at 30–32°C by an inline solution heater and temperature controller (TC-344B, Warner Instruments, Hamden, CT, USA). MSNs were identified with a 40× water-immersion objective on an upright microscope equipped with differential interface contrast optics under infrared illumination (BX5IWI, Olympus, Tokyo, Japan) and video observation (C3077-71 CCD camera, Hamamatsu Photonics, Japan). Current- and voltage-clamp recordings were made from MSNs in the NAc core with a MultiClamp 700A amplifier (Molecular Devices, Sunnyvale, CA, USA). Only MSNs having a resting membrane potential more negative than −65 mV and spike amplitude higher than 55 mV were used for experiments. Electrodes were made using borosilicate glass micropipettes (Warner Instruments) prepared with a P-97 Flaming–Brown micropipette puller (Sutter Instruments, Novato, CA, USA). Pipettes filled with internal solution (containing, mM: 145 potassium gluconate, 2 $MgCl_2$, 0.1 EGTA, 2 Na_2ATP, and 10 Hepes; pH 7.2 with KOH; 290 mosmol l^{-1} adjusted with sucrose) displayed resistance of 3–5 MΩ. Access resistance was monitored throughout the recording and was typically <15 MΩ. Data were not corrected for the liquid junction potential (−16 mV).

In a set of experiments aimed at studying the excitability of MSNs the perforated-patch configuration was used. For these recordings, gramicidin (Sigma) was added to the pipette solution (the same as in whole-cell recordings) at 10 μg ml^{-1}. Gramicidin was first dissolved in dimethylsulphoxide (DMSO) to a concentration of 10 mg ml^{-1} and it was freshly made every 2 h. Stock

solutions were then diluted in the pipette solution just before use. Before backfilling the pipette with the gramicidin-containing solution, the pipette tip was filled with gramicidin-free pipette solution by brief immersion. Gigaseals were formed with little or no suction to avoid break-in; perforation began within 5–10 min, developing steadily for the following 10–20 min. The progress of perforation was evaluated by monitoring the access resistance. When it had reached a steady level around 30 MΩ or lower, the recording was started. Access resistance was carefully monitored throughout the experiment, and any neurons in which a sudden drop in this parameter occurred were discarded. Only cells exhibiting stable firing discharge for at least 5–10 min under control condition were used for this set of experiments.

In some experiments membrane input resistance was evaluated in current-clamp mode using series of 600 ms hyperpolarizing steps (from −60 to 0 pA in 20 pA increments). Input resistance was calculated from the peak voltage achieved at each step. The input resistance values were derived from the linear portion of the intensity-to-voltage (I–V) relationship as the slope of the linear regression fitting line calculated by using the Clampfit program (pCLAMP9 software, Molecular Devices).

Data acquisition and stimulation protocols were performed by Digidata 1200 Series interface and pCLAMP 9 software. Data were filtered at 1 kHz and digitized at 10 kHz.

In the experiments presented in Fig. 9, a bipolar tungsten electrode (Warner Instruments) was used to stimulate excitatory afferents projecting onto MSNs (10 Hz). The stimulating electrodes were positioned 200–300 μm rostral to the recording electrode.

To isolate persistent Na^+ current (I_{NaP}) in whole-cell voltage-clamp recordings, we used a modified aCSF containing 20 mM tetraethylammonium chloride (TEA) and 0.2 mM $CdCl_2$. The voltage dependence of I_{NaP} was determined using standard protocols (Yue *et al.* 2005). The following equation was used to convert the ramp current to conductance $G(V)$:

$$G(V) = I(V)/(V - V_{Na}) \quad (1)$$

where V_{Na} is the Na^+ reversal potential, V the ramp potential, and $I(V)$ the peak current amplitude. G_{max} was extrapolated as the maximal Na^+ conductance; V_{50} was also extrapolated as the membrane voltage (V) at which $G(V)$ is 50% of G_{max}.

Statistical analysis. Data are expressed as means ± S.E.M. Statistical significance was assessed with Student's paired t test. For experiments involving fewer than 12 observations, Wilcoxon's signed-rank test (for paired data) and the Mann–Whitney test (for unpaired data) were used. Chi-square test was used to determine if the proportion of cells affected by DHPG differed under different conditions. For all statistical evaluations a P value < 0.05 was considered significant.

Drugs. Drugs were diluted to working concentrations in oxygenated aCSF before use or applied intracellularly through the recording pipette. A three-way stop-cock connected to the perfusion inlet tube was used to introduce test-drug solutions into the chamber containing the brain slice. The following drugs were purchased from Tocris Bioscience (Bristol, UK): (*RS*)-3,5-dihydroxyphenylglycine (DHPG), 2-methyl-6-(phenylethynyl)pyridine hydrochloride (MPEP), 1-[6-[[(17b)-3-methoxyestra-1,3,5(10)-trien-17-yl]amino]hexyl]-1H-pyrrole-2,5-dione (U-73122), 2-[2-[4-(4-nitrobenzyloxy)phenyl]ethyl] isothiourea mesylate (KB-R7943), 2-amino-6-trifluoromethoxybenzothiazole hydrochloride (riluzole), 2,3-dioxo-6-nitro-1,2,3,4-tetrahydrobenzo[f]quinoxaline-7-sulfonamide disodium salt (NBQX), and D-(−)-2-amino-5-phosphonopentanoic acid (D-AP5). The following drugs were purchased from Sigma: kynurenic acid, picrotoxin, TEA, guanosine 5′-[β-thio]diphosphate trilithium salt (GDPβS), L-β-threo-benzyl-aspartate (TBOA), 1-*O*-octadecyl-2-*O*-methyl-sn-glycero-3-phosphorylcholine (ET-18-OCH_3), ethylenedioxybis(*o*-phenylenenitrilo)tetraacetic acid (BAPTA), DL-fluorocitric acid. Tetrodotoxin was purchased from Alomone Laboratories (Jerusalem, Israel). [*N*-(4-Chlorobenzyl)]2,4-dimethylbenzamyl (CB-DMB), was a gift from Prof. L. Annunziato (Federico II University of Naples, Italy). All stock solutions were made with distilled water except for riluzole, KB-R7943, U-73122, MPEP, CB-DMB and picrotoxin, which were dissolved in DMSO.

DL-Fluorocitric acid was prepared as described previously by Martín *et al.* (2007). Briefly, the barium salt of DL-fluorocitric acid was first dissolved in 0.1 M HCl, and the barium was precipitated from the solution with the addition of 0.1 M Na_2SO_4. This solution was then buffered (0.1 M NaH_2PO_4) and centrifuged at 800 *g* for 10 min. The supernatant containing fluorocitrate was removed and added to aCSF to a final concentration of 1 mM. The slices were incubated in gassed aCSF plus fluorocitrate for 1 h and then continuously perfused thereafter during the experiment with the same solution.

Alexa Fluor 568 (Invitrogen, Carlsbad, CA, USA) (100 μM) was added to the intracellular solution to morphologically identify recorded neurons. Z-stacks of confocal images were acquired after dye excitation at 543 nm with a Prairie confocal microscope (Prairie Technologies, Middleton, WI, USA).

Results

mGluR5 activation enhances MSN excitability

Patch-clamp recordings were performed from GABAergic MSNs, which represent >90% of the neurons in the NAc. These cells, whose general properties are shown in Fig. 1*A*, displayed a resting membrane potential of -70.4 ± 1.1 mV ($n = 68$), inward rectification at a hyperpolarized membrane potential, ramp depolarization at subthreshold levels, and regular AP firing when stimulated with over-threshold voltages. The electrophysiological and morphological features of the recorded cells (Fig. 1*B*) are consistent with those reported for MSNs (Hopf *et al.* 2003; Dong *et al.* 2006). A few cells (∼2%) exhibited large, fast afterhyperpolarizations and higher discharge rates than those of most cells – features that are typical of fast-spiking GABAergic interneurons (Plenz & Kitai, 1998). They were excluded from further investigation.

Group I mGluR activation has been shown to cause membrane depolarization in different brain regions (Sekizawa & Bonham, 2006; Huang & van den Pol, 2007). Before investigating the impact of mGluR5 activation on MSN firing, we therefore studied the effects of class I mGluR activation on the resting conductances of these neurons. Slice superfusion with DHPG (20–40 μM) caused mild depolarization (3.2 ± 0.8 mV, $n = 6$; $P < 0.05$) from a resting membrane potential of -70 ± 0.4 mV. In voltage-clamp recordings performed at a holding potential of -70 mV, bath application of 40 μM DHPG elicited slow, tonic, inward currents (-22.6 ± 1.3 pA; $n = 40$; Fig. 1*C*) that were associated with increased noise levels. To pharmacologically characterize this current the effects of DHPG were studied before and after application of different compounds. However, before testing the effects of the different pharmacological agents the possible occurrence of receptor desensitization was assessed in control experiments in which a single cell was exposed to two consecutive applications of DHPG at 10–15 min intervals. The currents elicited by the two drug applications had similar amplitudes (-20.7 ± 2.1 and -20.8 ± 2.6 pA, respectively; $n = 6$; $P > 0.3$). We then tested the effects of the selective mGluR5 antagonist MPEP (50 μM) that reduced the DHPG-induced current amplitude by $84 \pm 4\%$ (from -21.1 ± 2.8 to -3.2 ± 0.6 pA; $n = 6$; $P < 0.001$; Fig. 1*D*).

In hippocampal neurons, Fellin *et al.* (2006) described a tonic NMDA-receptor-mediated current caused by glutamate release from astrocytes following P2X-receptor activation. However, the DHPG-induced tonic current in NAc MSNs was unaffected by slice exposure to either the NMDA-receptor antagonist D-AP5 (50 μM), or Mg^{2+}-free aCSF (Fig. 1*C*). To further assess the possible contribution of astrocytic mGluR5 activation in triggering tonic current in MSNs, we used the glia-specific metabolic inhibitor, fluorocitrate (Largo *et al.* 1996; Martin *et al.* 2007). We found that slice pre-incubation with 1 mM fluorocitrate did not prevent the tonic inward current elicited by DHPG (-20.3 ± 3.7 pA, $n = 7$), thus indicating that glial cells are not involved in our effects. In contrast, the tonic current was significantly reduced to -12.2 ± 2.2 pA ($n = 5$; $P < 0.05$) following dialysis of MSNs with the G-protein blocker GDPβS (1 mM).

All these data indicate that DHPG effects are likely to be mediated by activation of neuronal mGluR5.

Current-clamp experiments were performed to determine whether the tonic inward current was associated with changes in membrane input resistance. When the DHPG effects had fully developed, hyperpolarizing currents were injected to bring the membrane potential to -70 mV. Starting from this holding current level, 600 ms hyperpolarizing steps (from -60 to 0 pA in 20 pA increments) were applied and the peak voltage achieved at each step was measured. The results of these experiments showed that, at membrane potentials subthreshold for Na^+ current activation (ranging from -70 to -85 mV), there were no changes in membrane input resistance (270.5 ± 13.5 MΩ during DHPG application *vs.* 268.5 ± 13.7 MΩ in controls), thus suggesting that the recorded current is not due to ion channel opening or closure.

A recent study has shown that in second-order baroreceptor neurons, DHPG-induced membrane depolarization associated with increased recording-noise is mediated by the activation of inward currents flowing through the Na^+/Ca^{2+} exchanger (Sekizawa & Bonham, 2006). Our findings are consistent with these observations. As shown in Fig. 1*E* (lower trace), the DHPG-induced tonic current in our NAc slices was clearly attenuated (-4.0 ± 1.4 pA *vs.* -20.6 ± 2.9 pA in controls; $n = 8$; $P < 0.001$) by exposure to the Na^+/Ca^{2+} exchanger blocker, KB-R7943 (100 μM, 5–10 min).

In another set of experiments slices were pre-incubated with a different Na^+/Ca^{2+}-exchanger blocker, the amiloride derivative CB-DMB (5 μM for 10–15 min; Bkaily *et al.* 1998; Annunziato *et al.* 2004; Jeffs *et al.* 2007; Tortiglione *et al.* 2007), which also significantly reduced the DHPG-induced tonic current (-8.6 ± 1.3 *vs.* -24.4 ± 2.3 pA in controls; $n = 10$; $P < 0.001$; Fig. 1*E*).

In the presence of KB-R7943, DHPG also increased the frequency and the amplitude of mEPSCs without significantly affecting their shape. These effects were never observed when DHPG was applied alone or in the presence of CB-DMB.

At this point, we were ready to assess the impact of mGluR5 activation on MSN spike firing – the primary aim of our study. To test the firing properties of MSNs during continuous depolarization, we exposed these cells to a series of 800 ms current pulses (one every 60 s) during whole-cell perforated-patch recordings. The amplitude of current pulse was increased from

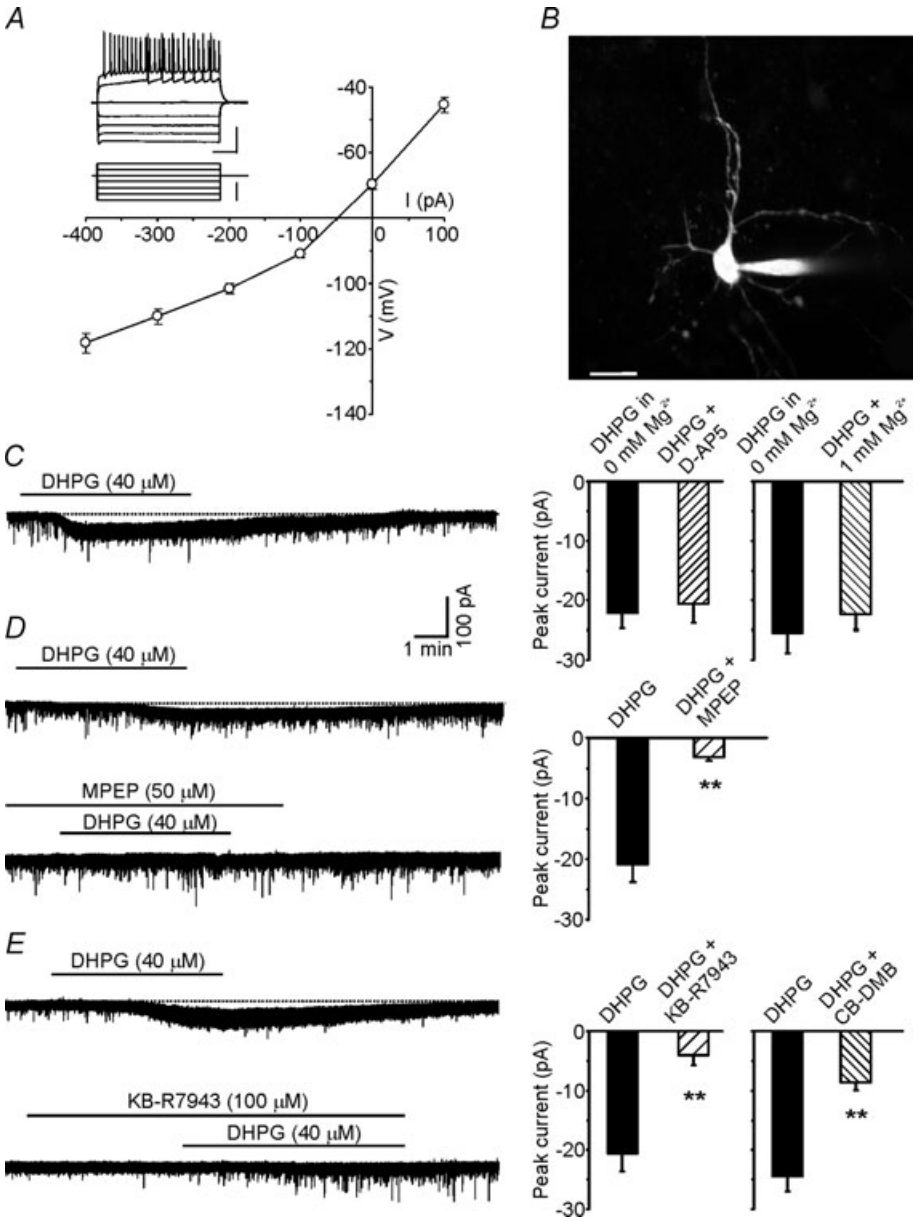

Figure 1. mGluR5 activation induces a small tonic current in MSNs
A, current-to-voltage relationship. Membrane potential at steady-state was plotted against the injected current amplitude ($n = 12$). Note inward rectification at hyperpolarized potentials. Inset, representative traces of an MSN response to hyperpolarizing and depolarizing current steps (bottom traces). Inset scale bars: 40 mV; 200 ms; 300 pA. *B*, morphology of an MSN revealed by dialysing the fluorescent dye Alexa 568 through the patch pipette. The image is the Z-projection of 27 planes. Scale bar: 15 μm. *C*, left, representative trace recorded in the voltage-clamp configuration showing the inward current elicited by 40 μM DHPG. Right, bar graph summarizing the effects of NMDA receptor blockade on DHPG-induced inward current. Each tested neuron was exposed first to DHPG in aCSF containing 0 mM Mg^{2+} and then to DHPG in aCSF containing either D-AP5 (50 μM; $n = 5$) or 1 mM Mg^{2+} ($n = 4$). *D*, left, blockade of mGluR5 activity by exposure to 50 μM MPEP inhibited the DHPG-induced inward current in MSNs. Right, bar graph showing the mean amplitudes of currents evoked by DHPG applied alone and in the presence of MPEP ($n = 6$). Each tested neuron was exposed first to DHPG (to verify its sensitivity to this agonist) and then to DHPG plus MPEP. After whole-cell dialysis with GDPβS (1 mM), the amplitude of the DHPG-induced tonic current was significantly reduced ($n = 7$). *E*, the DHPG-induced current in MSNs was attenuated by inhibition of Na^+/Ca^{2+}-exchanger with KB-R7943 (100 μM; $n = 8$) and CB-DMB (5 μM; $n = 10$). Each tested neuron was exposed first to DHPG and then to DHPG plus KB-R7943 or CB-DMB. Error bars indicate S.E.M., $^*P < 0.05$, $^{**}P < 0.001$ in this as well as in the following figures.

−50 pA (hyperpolarizing) to 150 pA (depolarizing, both subthreshold and suprathreshold for APs) in 50 pA steps. The DHPG-induced membrane depolarization mediated by the Na^+/Ca^{2+} exchanger obviously increases the spike firing of MSNs as it brings their membrane potential closer to the threshold for action potential firing. To determine whether DHPG has the potential to affect spike firing independently of this effect, during these experiments we counteracted the Na^+/Ca^{2+}-exchanger-dependent depolarization by injecting hyperpolarizing currents that kept the membrane potential at −70 mV during interpulse intervals. Under these experimental conditions, bath application of 40 μM DHPG significantly increased the number of APs compared with that observed under control conditions ($+25.3 \pm 10.1\%$; $n = 5$; $P < 0.001$; Fig. 2). The spike-firing enhancement developed quite slowly and peaked ∼5–6 min after application of DHPG. Thirty minutes after DHPG washout, the MSNs retained some degree of hyperexcitability reflected by a small increase ($+6.4 \pm 9.0\%$) in the number of spikes compared with that seen at baseline. Increased spike firing was associated with a modest but significant decrease in the latency of the first AP (from 150 ± 3 to 130 ± 3 ms; $P < 0.05$).

Slice pre-treatment with the selective mGluR5 antagonist MPEP (50 μM for 5 min; $n = 4$) completely abolished the DHPG-induced increase in spike firing, suggesting that this effect is mediated by activation of mGluR5.

mGluR5 activation induces afterdepolarization in MSNs

The next set of experiments was designed to identify the mechanisms underlying the mGluR5-mediated effects on spike firing. In many neurons APs are followed by hyperpolarizing or depolarizing afterpotentials, which regulate cell excitability for periods ranging from a few milliseconds to several seconds. Afterpotentials following a single spike or spike train can mediate different forms of feedback-based regulation of excitability (Bean, 2007; Beck & Yaari, 2008). In hippocampal CA1 pyramidal neurons and layer V cortical neurons, group I mGluR agonists cause long-lasting hyperexcitability by suppressing afterhyperpolarizations (AHP) (Ireland & Abraham, 2002; Sourdet *et al.* 2003). We wondered whether this mechanism might be involved in the DHPG-induced changes in excitability we observed in MSNs. In accordance with standard protocols, a train of four APs were elicited in MSNs by the application of four 2 ms depolarizing current pulses (1 nA; 10 ms pulse interval). At voltages between −70 and −60 mV, AHPs were never recorded under control conditions, but in the presence of DHPG an afterdepolarization (ADP) appeared in 23 of the 25 cells tested (Fig. 3). In 12 of these 23 MSNs, the ADP appeared as a slow phase of repolarization at the end of the spike train (Fig. 3*A*). In the other 11 cells, the trajectory of the post-AP voltage trace had a clear rising phase (Fig. 3*B*). The average ADP decay time was 658 ± 78 ms ($n = 23$), and the time-to-peak was 149 ± 26 ms ($n = 11$). The latter variable was measured only when there was a clear rising phase between the end of repolarization and the ADP peak.

At membrane potentials ranging between −70 and −60 mV, we calculated the amplitude of the DHPG-induced ADP, relative to the membrane potential before the current injections, by averaging the membrane potential values 15 ms before and after the ADP peak. The mean amplitude was 7.7 ± 0.6 mV ($n = 23$; $P < 0.001$; Fig. 3*E*), and effects were fully reversed by a 5–10 min drug washout.

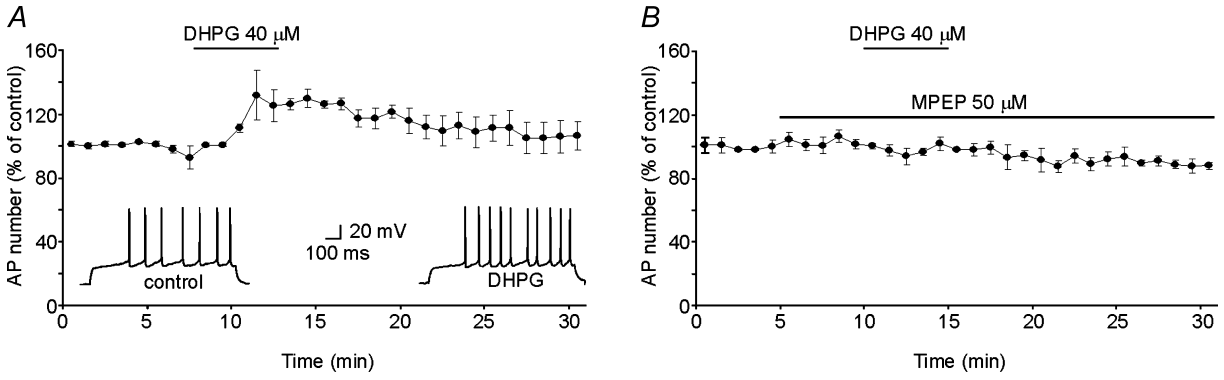

Figure 2. Selective mGluR5 activation increases the excitability of MSNs
A, normalized changes in the number of APs before, during, and after 5 min cell exposure to 40 μM DHPG ($n = 5$). Insets, perforated patch-clamp recordings from an MSN in the current-clamp configuration showing the increase in number of APs elicited by DHPG. The AP trains were evoked by an 800 ms depolarizing current injection (0.1 nA). To avoid increased excitability due to membrane depolarization resulting from the activation of Na^+/Ca^{2+} exchanger, we used a hyperpolarizing current injection to keep the membrane potential at −70 mV during the interpulse intervals. *B*, mGluR5 blockade with 50 μM MPEP prevented the DHPG-induced increase in the number of APs ($n = 4$).

Next, to evaluate the voltage dependence of the DHPG-induced ADPs, we injected negative or positive currents into MSNs to produce membrane potentials ranging from −90 to −50 mV (at ∼10 mV intervals). Figure 3*C* shows examples of the ADPs recorded at different potentials in one of these cells. The ADP amplitude was clearly voltage dependent, with maximum effects at prespike potentials ranging from −55 to −70 mV (Fig. 3*D*). The ADP was absent at more negative potentials near E_K. At membrane potentials less negative than −50 mV, ADPs could not be measured because of the appearance of AP firing.

The DHPG-induced ADP was markedly inhibited by slice pre-incubation with MPEP (1.1 ± 0.4 mV; $n = 8$; $P < 0.001$; Fig. 3*F*), so – like the DHPG-induced increase in spike firing – this effect seems to be mediated by mGluR5 activation.

DHPG also activated the Na^+/Ca^{2+} exchanger, and we wondered whether this mechanism was involved in its ability to induce ADP. Slice incubation for 5–10 min

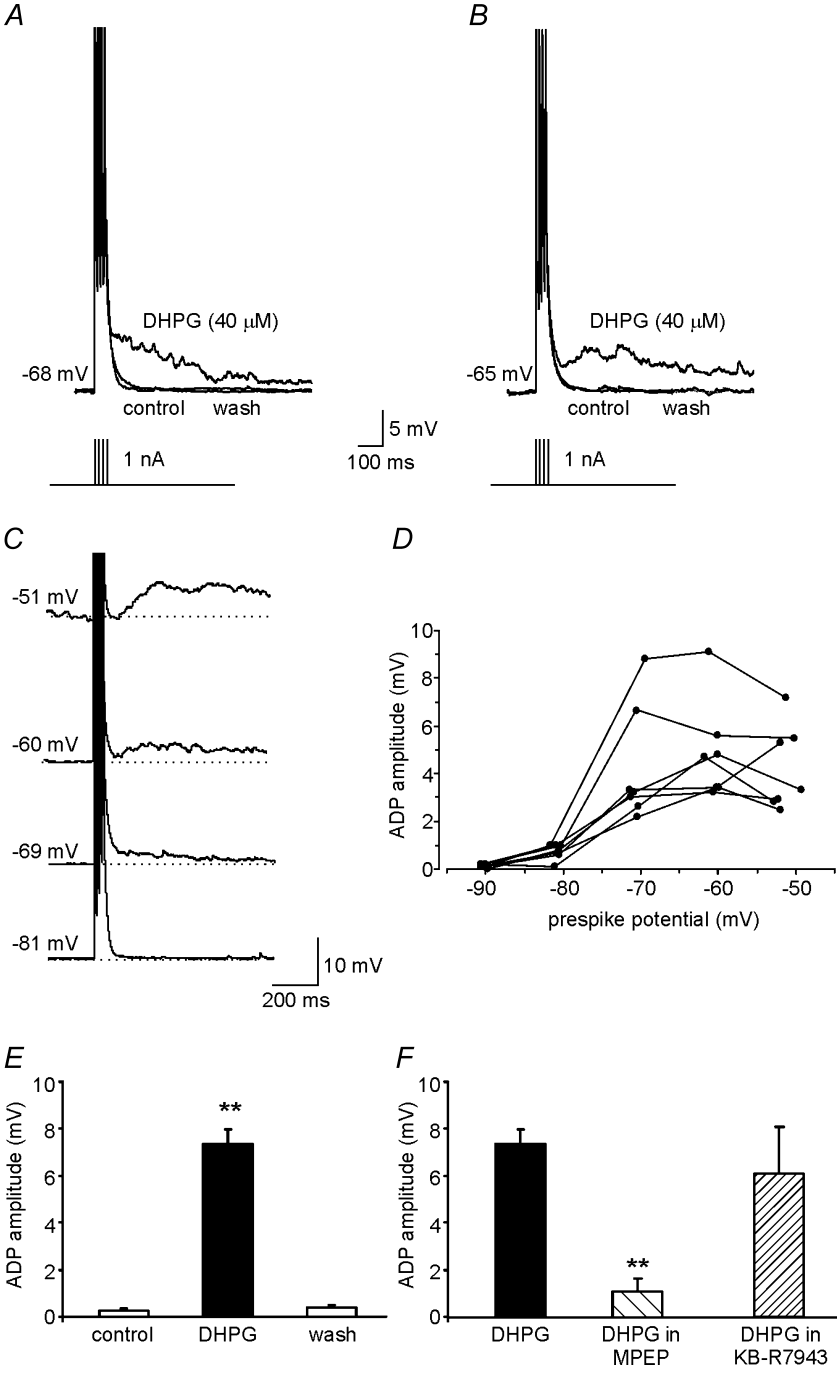

Figure 3. mGluR5 activation induces afterdepolarizations in MSNs
A and *B*, two representative whole-cell, current-clamp recordings showing ADPs induced by exposure to 40 μM DHPG. In *A*, the ADP appears as slow phase of repolarization whereas the ADP in *B* has a clear rising phase. A train of four APs (100 Hz) was elicited by current injection (1 nA for 2 ms) to evoke afterpotentials. *C*, representative examples of ADPs recorded in MSNs maintained at different membrane potentials by current injection. *D*, relation of ADP amplitude to membrane potentials for each of the 7 cells tested. *E*, mean ADP amplitude ($n = 23$) under control conditions, in the presence of DHPG, and following DHPG washout. *F*, mean amplitude of the DHPG-induced ADP in the presence of MPEP (50 μM; $n = 6$) and KB-R7943 (100 μM; $n = 4$).

with the Na^+/Ca^{2+} exchanger inhibitor KB-R7943 (100 μM) had no significant effect on the amplitude of the ADP elicited by DHPG (6.1 ± 2.0 mV; $n = 4$; Fig. 3*F*), suggesting that the tonic inward current and ADP are independent effects of mGluR5 activation in MSNs.

Our next objective was to identify the intracellular pathway by which mGluR5 activation induces ADP. In particular, we determined whether G-protein-dependent PLC activation and Ca^{2+} signalling are responsible for the DHPG-induced ADP. The effects of DHPG were thus tested in MSNs dialysed for 5–10 min with GDPβS (1 mM), which blocks G-protein-signalling; the PLC inhibitor U-73122 (1 μM); or the calcium chelator EGTA (5 mM). All these treatments markedly reduced the size of the ADP (to 1.5 ± 0.4, $n = 6$; 1.7 ± 0.5, $n = 5$; and 0.5 ± 0.2 mV, $n = 7$, respectively) (Fig. 4). Because U-73122 is a potent but not highly selective PLC inhibitor, in another set of experiments slices were pre-incubated with a different PLC-inhibitor, ET-18-OCH_3 (10 μM, Horowitz *et al.* 2005), for 15–30 min prior to DHPG administration. ADP amplitude was significantly reduced by this treatment to 1.5 ± 0.3 mV ($n = 5$; Fig. 4*B*), similarly to what we observed with U-73122. Taken together, these data suggest that mGluR5-dependent ADPs in MSNs are mediated by G-protein/PLC/Ca^{2+} signalling.

Although intracellular calcium is required for ADP generation, Ca^{2+} influx during APs does not seem to play a role. Indeed, DHPG still induced ADP during cell perfusion with low-Ca^{2+} aCSF and after the blockade of voltage-gated Ca^{2+} channels with 0.2 mM $CdCl_2$ (data not shown).

Persistent Na^+ current (I_{NaP}) contributes to mGluR5-dependent ADP

Voltage-clamp recordings were performed to explore the nature of the current underlying the DHPG-induced ADP. The protocol was designed to reproduce the stimulus used in current-clamp experiments (four short, square-wave depolarizing steps from -65 to $+20$ mV; 2 ms duration, 10 ms pulse interval). As shown in Fig. 5*A* in a representative MSN held at -65 mV, when this stimulation protocol was applied in the presence of DHPG, an inward current with kinetics compatible with ADP was recorded. This current had a mean amplitude of -22.1 ± 2.7 pA ($n = 13$) and a mean decay time of 125 ± 51 ms. The latter value is lower than that observed in current-clamp recordings but this discrepancy is not surprising because ADP decay time is shaped by the time constant of the cell membrane. Moreover, the stimulation protocol used in the voltage-clamp recordings does not reproduce exactly the voltage excursion experienced by the cell in current-clamp conditions.

Current-to-voltage curves based on data collected before and during exposure to DHPG were analysed to determine whether these currents were voltage dependent. Membrane potential was increased in 10 mV steps from a holding potential of -65 mV to voltages between -85 and -55 mV. The net current activated by DHPG was measured by subtracting the current recorded under control conditions from that recorded in the presence of the drug (Fig. 5*B*, $n = 8$). As previously observed in our current-clamp recordings, the net inward current was absent at very hyperpolarized potentials.

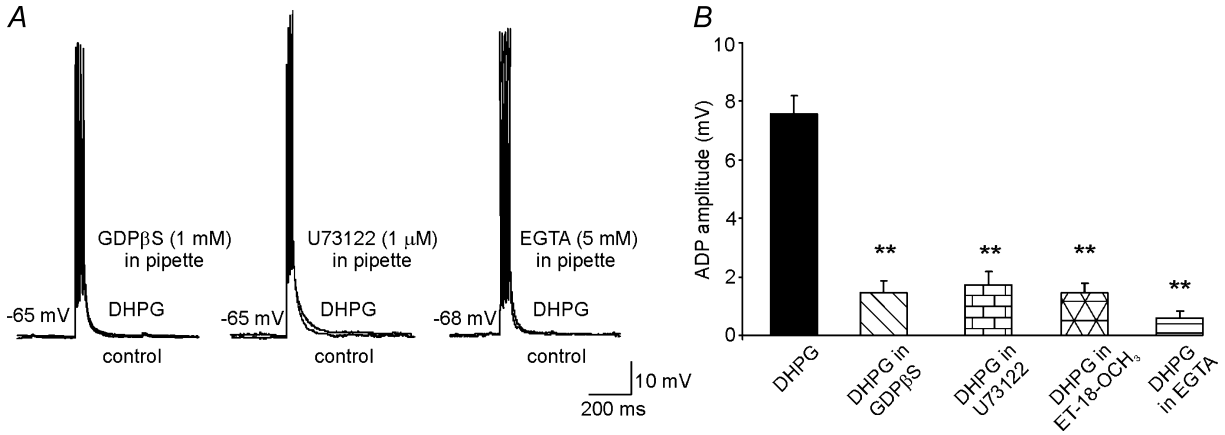

Figure 4. G-protein, PLC and intracellular Ca^{2+} are required for the DHPG-induced ADP
A, representative DHPG-induced ADPs recorded under the following experimental conditions: blockade of G-protein by GDPβS (1 mM; $n = 6$); blockade of phospholipase C by U73122 (1 μM; $n = 5$); and reduction of intracellular Ca^{2+} by EGTA (5 mM; $n = 7$). GDPβS, U73122 and EGTA were applied intracellularly through the recording pipette. *B*, mean amplitude of ADP in the different experimental conditions.

To determine whether the observed inward currents were due to activation or inhibition of ionic conductances in MSNs, we applied a voltage step of −5 mV before and during the DHPG-induced effects. In the latter condition, currents induced by the voltage step command were increased from 16.0 ± 2.4 to 22.4 ± 2.3 pA (+44.5 ± 7.8%; $n = 5$). The conductance increase documented in these experiments indicates that the DHPG-induced inward current is mediated by ion channel opening.

The possible involvement of voltage-gated Na^+ channels in the inward currents induced by DHPG was then assessed. When slices were preincubated with a selective blocker of these channels, TTX (0.5 μM), the

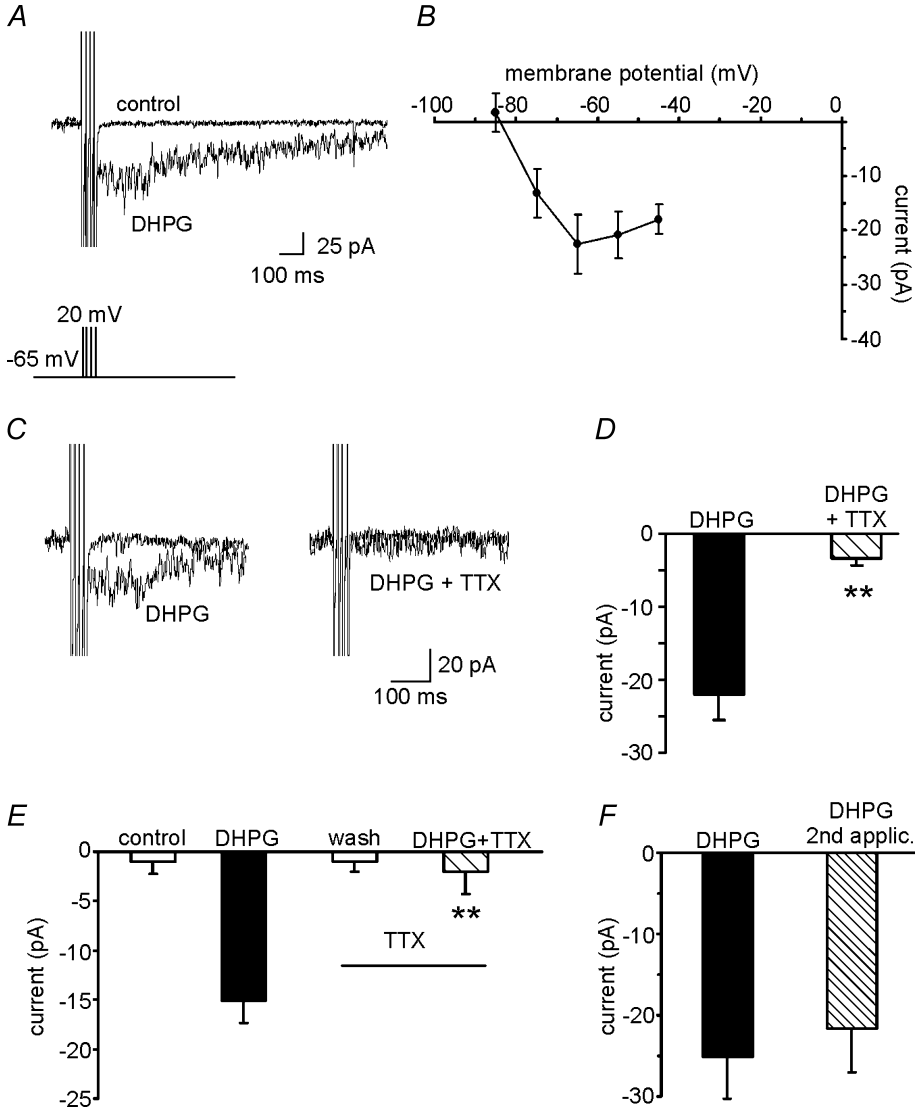

Figure 5. ADP is mediated by an inward Na^+ current
A, representative traces showing the DHPG-induced inward current. The voltage-clamp protocol was designed to reproduce the stimulus used in current-clamp experiments (i.e. four short, square-wave depolarizing steps from −65 to +20 mV, 2 ms pulse duration). *B*, current-to-voltage relationships based on data collected from slices perfused with DHPG. Net currents activated by DHPG at the various voltages were obtained by subtracting currents recorded under control conditions from those recorded in the presence of DHPG. Voltage steps (from −85 to −45 mV in 10 mV increments) were applied from holding potential of −65 mV. *C*, representative traces from two different set of experiments showing that the DHPG-induced inward current (left) is almost abolished in the presence of TTX (right). *D*, mean amplitude of the DHPG-induced inward currents in the two different conditions. *E*, bar graph showing the mean amplitude of currents induced by two consecutive applications of DHPG (alone and in the presence of TTX) in the same MSN ($n = 4$). *F*, mean amplitude of inward currents induced by two consecutive DHPG applications. Note the absence of significant receptor desensitization during the second DHPG application ($n = 4$).

DHPG-induced inward currents were almost completely abolished (-3.4 ± 0.9 pA; $n = 9$ *vs.* -22.1 ± 2.7 pA in controls; $n = 13$; Fig. 5*C* and *D*). In other experiments, we compared the amplitudes of DHPG-induced currents recorded from the same cell before and after application of 0.5 μM TTX. The results (Fig. 5*E*) confirmed TTX's marked inhibitory effects on the current elicited by DHPG (-2.0 ± 2.3 *vs.* -15.1 ± 2.1 pA; $n = 4$; $P < 0.001$). The possible role of receptor desensitization in these findings was excluded in control experiments, in which a single cell was exposed to two consecutive applications of DHPG in the absence of TTX. As shown in Fig. 5*F*, the currents elicited by the two drug applications had similar amplitudes ($n = 4$).

The effects of TTX on DHPG-induced ADP were also investigated in current-clamp experiments. Control ADP responses were first elicited in normal aCSF. The cell was then allowed to recover from DHPG exposure in the presence of TTX; after 5 min DHPG was re-applied. Because TTX prevented AP firing, the amplitude of the injected current pulses used during the second exposure was increased to 2 nA producing capacitive changes in the membrane potential that mimicked APs. Under these conditions, TTX reduced the ADP amplitude to 0.6 ± 0.2 mV ($n = 5$; Fig. 6). Collectively, these data suggest that recruitment of TTX-sensitive Na^+ spike after-currents plays an essential role in the DHPG-induced ADPs we observed in MSNs.

In addition to the classical transient Na^+ current (I_{NaT}) responsible for AP generation, the voltage-dependent Na^+ currents also include persistent and resurgent types (I_{NaP} and I_{NaR}, respectively). These currents, which are active in the sub- and near-threshold ranges, have different kinetics, and they exert major effects on the excitability and signal processing of central neurons (Bean, 2007). Either or both of these currents could contribute to the DHPG-induced TTX-sensitive Na^+ spike aftercurrent. We choose to evaluate the involvement of the I_{NaP} because the I_{NaR} is characterized by fast inactivation kinetics, and it seems unlikely that a current of this type is responsible for membrane depolarization lasting hundreds of milliseconds.

The I_{NaP} in MSNs of the NAc has never been investigated. Therefore, before exploring its responses to mGluR5 activation, we attempted to identify the biophysical and pharmacological properties of this currents. When the I_{NaT} were inactivated by application of slow (50 mV s^{-1}) depolarizing voltage ramps from -70 to 0 mV, a net inward current was elicited in the MSNs at potentials ranging from -50 to 0 mV. The fact that this current was completely abolished by TTX (Fig. 7*Aa*) allowed us to identify it as I_{NaP} (French *et al.* 1990). Subtraction of the current traces obtained before and after TTX application yielded the current's 'pure' I_{NaP} component (Fig. 7*Ab*). The activation threshold of the I_{NaP} was approximately -50 mV, and current amplitude increased with depolarization, reaching maximal values at ~ -20 mV.

I_{NaP} current-to-voltage relationships were converted to conductance-to-voltage plots (Yue *et al.* 2005; eqn (1); Fig. 7*Ac*) from which G_{max} and V_{50} were extrapolated (0.8 ± 0.1 nS; -33.6 ± 1.0 mV; respectively; $n = 12$).

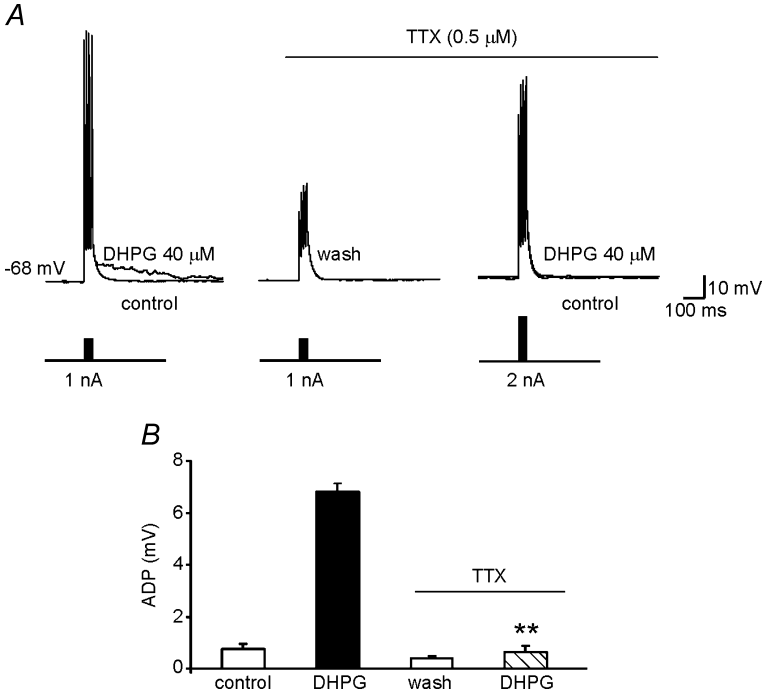

Figure 6. ADP is abolished by selective blockade of sodium conductances
A, in current-clamp recordings, application of the protocol described in Fig. 3 (four brief depolarizing current pulses, 1 nA, 2 ms) was associated with the usual response to DHPG (left). After DHPG washout (middle), a second DHPG application elicited no response in the presence of TTX (0.5 μM) even when we used higher-amplitude current pulses (2 nA) to compensate changes in membrane potential (right). *B*, summary of data on ADP amplitudes observed under the conditions described in *A*.

Because riluzole and 20 nM TTX have been shown to block I_{NaP} in many central neurons (Pace *et al.* 2007; Koizumi & Smith, 2008), we tested their effects on the inward current elicited in MSNs by depolarizing voltage ramps. As shown in Fig. 7*B*, I_{NaP} was almost completely abolished by both blockers: peak I_{NaP} current was inhibited by $86.2 \pm 5.2\%$ ($n = 5$; $P < 0.001$) and $89.6 \pm 2.7\%$ ($n = 5$; $P < 0.001$) after riluzole (Fig. 7*Bb*) and TTX treatments (Fig. 7*B*-*c*), respectively.

After characterizing the I_{NaP} in NAc MSNs, we tested the possible effects of DHPG on this current. First, we examined the influence of bath-application of DHPG

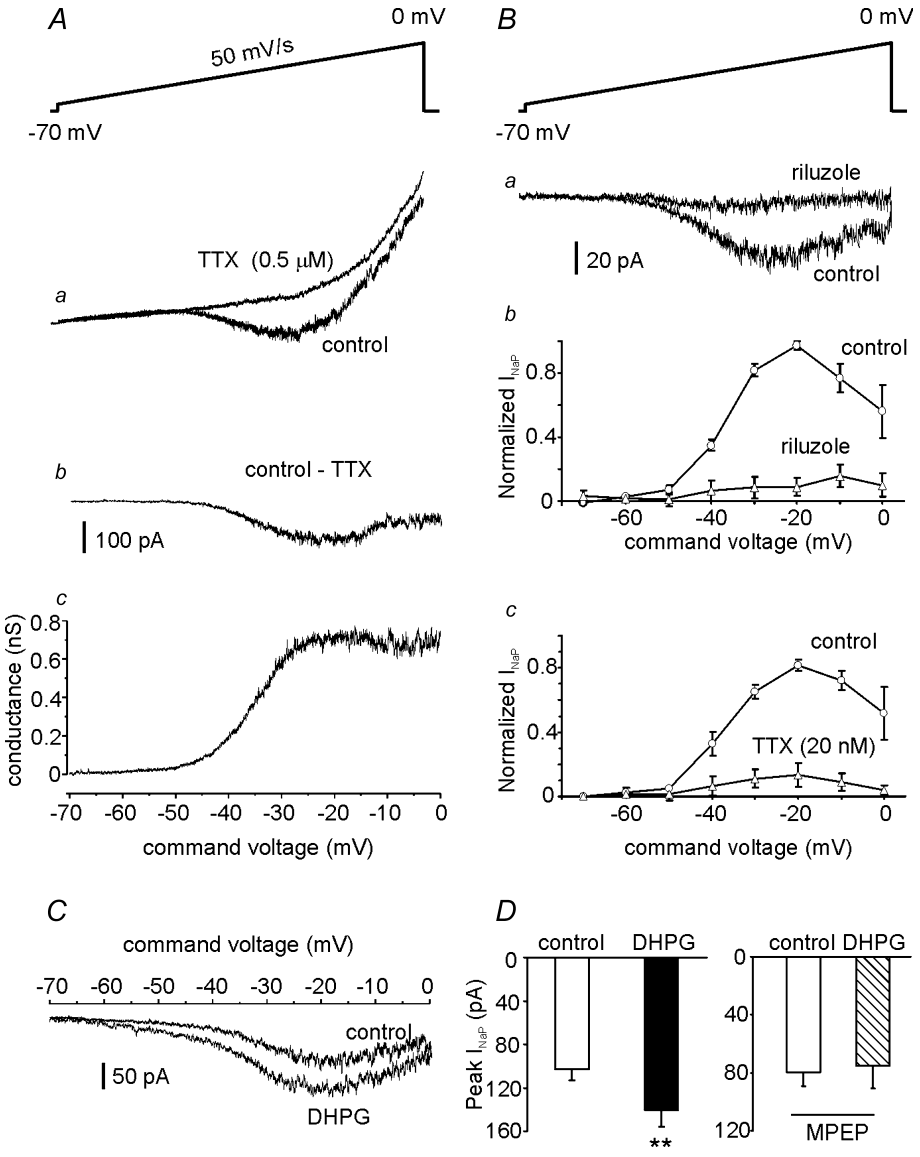

Figure 7. DHPG increases persistent sodium current (I_{NaP}) in MSNs
A and *B*, biophysical and pharmacological properties of I_{NaP} elicited in MSNs. Slices were perfused with aCSF containing 0.2 mM $CdCl_2$ (to block Ca^{2+} channels) and 20 mM TEA (to reduce K^+ current). *Aa*, instantaneous current–voltage curve during application of slow voltage ramps (50 mV s^{-1}; inset) before and during exposure to 0.5 μM TTX. *Ab*, I_{NaP} was isolated by digital subtraction of responses obtained in the presence of TTX from those recorded under control conditions. *Ac*, the subtracted current traces were converted to conductance (see Methods) and plotted against ramp voltage to obtain the I_{NaP} conductance–voltage relationship ($n = 14$). *Ba*, representative traces showing the effects of riluzole (10 μM) on I_{NaP}. Pooled results showing I_{NaP} evoked at different ramp potentials before and during riluzole exposure ($n = 5$), and before and during 20 nM TTX exposure (*Bc*, $n = 5$). *C*, representative traces (left) showing the I_{NaP} increase induced by DHPG application. *D*, bar graph showing the mean current amplitudes, measured at the peak of I_{NaP}, before and after DHPG application (left; $n = 5$). Slice pre-incubation for 5–10 min with MPEP prevented the DHPG-induced increases in I_{NaP} (right; $n = 4$).

on I_{NaP} at membrane potentials associated with ADP. As shown in Fig. 7*C*, the drug significantly augmented I_{NaP} at potentials between −60 and 0 mV. The peak I_{NaP} increased by 37.4 ± 15.2% (from −103 ± 10 to −140 ± 12 pA, $n = 5$; $P < 0.05$). It is noteworthy that the activation threshold of I_{NaP} (∼ −50 mV in controls) was left-shifted in the presence of DHPG to ∼–60 mV, a voltage quite similar to that recorded at the end of the spike downstroke and the beginning of ADP (−58.3 ± 0.8 mV; $n = 23$). The effects of DHPG were virtually abolished by MPEP ($n = 4$, Fig. 7*D*), confirming that they are due to mGluR5 activation.

The finding that mGluR5 activation increases I_{NaP} and induces TTX-sensitive ADP suggests that mGluR5-dependent ADPs are the result of I_{NaP} modulation. To verify this hypothesis, we studied DHPG-induced ADPs during selective I_{NaP} blockade. As shown in Fig. 8*A* and *B*, slice pre-exposure for 10 min to either 10 μM riluzole or 20 nM TTX significantly diminished the amplitude of these ADPs

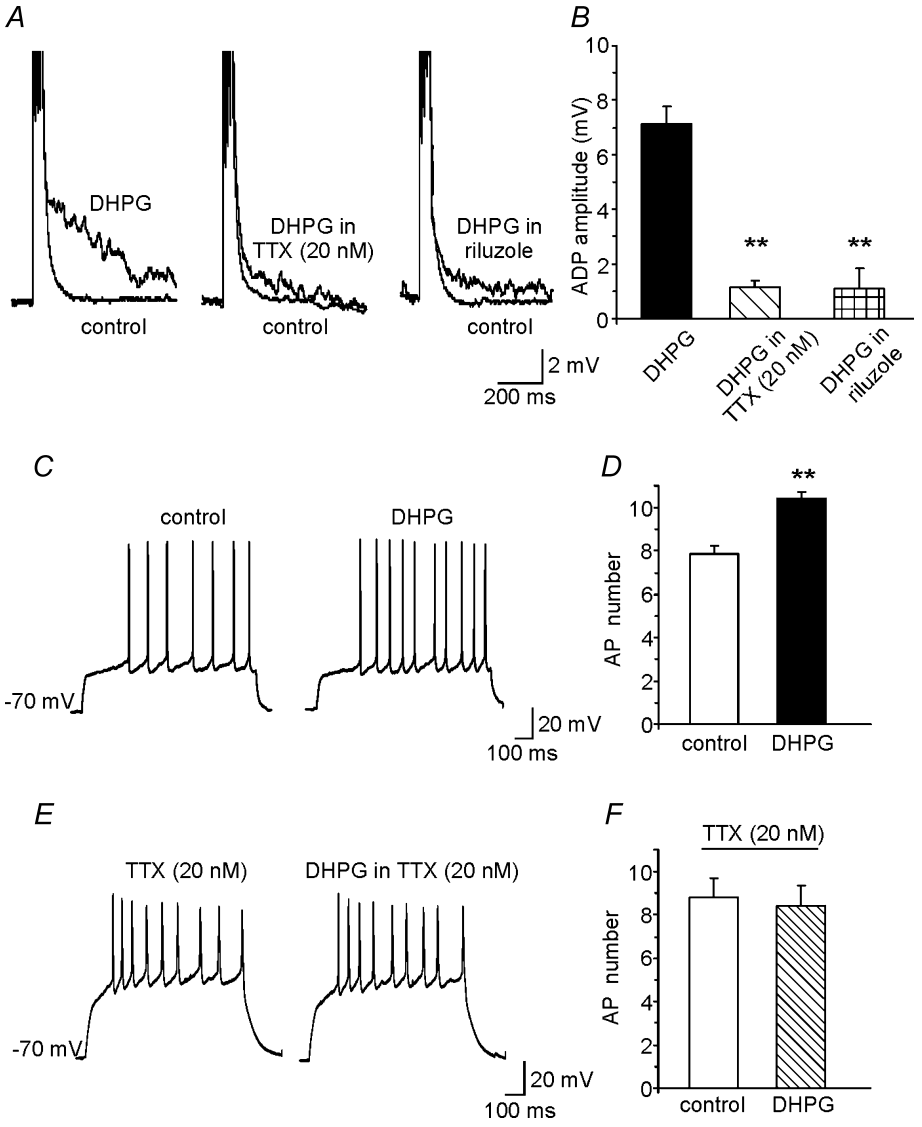

Figure 8. Selective blockade of I_{NaP} reduces the ADP and the increases in excitability induced by DHPG
A, representative traces of DHPG-induced ADP recorded in two different sets of experiments in which I_{NaP} was blocked by 20 nM TTX ($n = 5$) or riluzole ($n = 6$). ADP induced by DHPG in the absence of Na^+ channel blockers is shown for comparison on the left. *B*, mean amplitude of ADP under the experimental conditions shown in *A*. *C*, representative traces showing the increase in AP number induced by DHPG under the same experimental conditions shown in Fig. 2*A*. *D*, mean increase in AP number induced by DHPG in 5 cells. *E*, representative traces showing the absence of DHPG-induced increases in AP number when I_{NaP} was blocked by 20 nM TTX. *F*, mean number of APs in the presence of 20 nM TTX before (control) and after DHPG application ($n = 5$).

(1.1 ± 0.3 mV, $n = 7$; and 1.1 ± 0.2 mV, $n = 5$, respectively *vs.* 7.3 ± 3.1 mV in controls, $n = 23$).

We had now demonstrated that mGluR5 activation (1) increases MSN excitability, (2) elicits ADP, and (3) enhances the I_{NaP} suspected to cause ADP. Our next goal was to determine whether these effects were causally related. We reasoned that if mGluR5-dependent increases in I_{NaP} are the mechanism underlying ADP, and if ADP is responsible for the enhanced MSN excitability produced by mGluR5, I_{NaP} blockade should prevent DHPG from increasing MSN excitability. As shown in Fig. 8*C–F*, DHPG's effects on MSN firing were indeed annulled when the cells were exposed to 20 nM TTX ($n = 5$). We limited our investigation to the effects of TTX block of I_{NaP} because at the concentration used this drug has no significant effect on the I_{NaT} (Koizumi & Smith, 2008). Riluzole, in contrast, affects multiple types of K^+ channels, including the small- and large-conductance Ca^{2+}-activated K^+ channels (Wu & Li, 1999; Grunnet *et al.* 2001), which are known to influence AP shape and interspike potential.

Stimulation of glutamatergic afferents triggers mGluR5-dependent increase in excitability

Next, we focused on the role of mGluR5 activation in regulating the excitability of NAc MSNs under more physiological conditions. We hypothesized that glutamate released from glutamatergic terminals activates mGluR5 and triggers ADP thereby increasing MSN excitability. To test this hypothesis we first monitored the spike firing rate of MSNs during electrical stimulation of the prefrontal cortex glutamatergic afferents which represent the main excitatory pathway innervating the NAc together with projections arising from hippocampus and basolateral amygdala (Groenewegen *et al.* 1980). As in experiments shown in Fig. 2, we counteracted the Na^+/Ca^{2+}-exchanger-dependent membrane depolarization by injecting hyperpolarizing currents that kept the membrane potential at −70 mV during interpulse intervals. During these experiments, the slices were perfused with the ionotropic GABA-receptor blocker picrotoxin (100 μM), the AMPA-receptor antagonist NBQX (30 μM), and the NMDA-receptor antagonist D-AP5 (50 μM). Under these conditions, stimulation of the glutamatergic afferents (10 Hz, 100 s) significantly enhanced the excitability of 5 of the 6 MSNs tested, as shown by the increase in AP number from 6.4 ± 1.3 (in controls) to 10.2 ± 1.8 ($P < 0.05$). When 50 μM MPEP ($n = 4$) or 20 nM TTX ($n = 6$) was present in the aCSF, this increase was no longer seen (Fig. 9*B*). We also tested whether glutamate released following afferent stimulation was able to trigger ADPs. In 4 out of the 8 tested neurons ADP was recorded though its amplitude was much smaller than that induced by DHPG (1.2 ± 0.2 mV; Fig. 9*C*,*D*). To limit the reduction of glutamate concentrations at the synaptic level due to the activity of glutamate transporters located on both glial cells and neurons, we repeated these experiments in the presence of the non-specific glutamate transporter blocker TBOA (100 μM). Under these experimental conditions greater ADPs were observed (2.3 ± 0.5 mV, in 6 out of 13 neurons tested; Fig. 9*C* and *D*).

These data suggest that glutamatergic fibre stimulation induces ADP and enhances the neuronal excitability of MSNs via the synaptic activation of mGluR5.

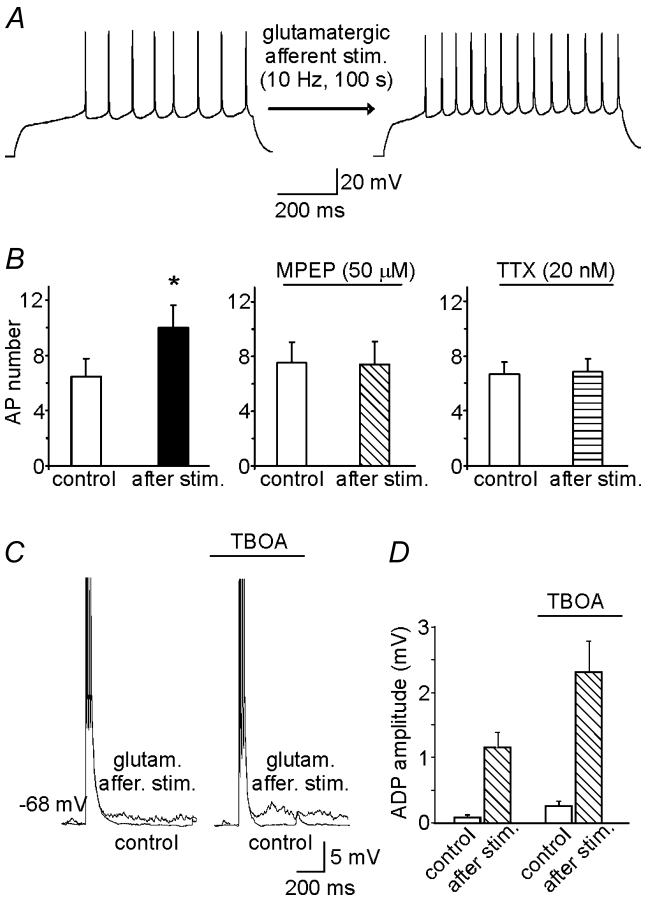

Figure 9. Glutamatergic afferent stimulation induces mGluR5-dependent increases in MSN excitability
A, representative traces showing the increase in the number of APs following glutamatergic afferent stimulation. Afferents were stimulated with a train of stimuli delivered at 10 Hz for 100 s. This experiment was performed in the presence of the glutamate ionotropic receptor antagonists NBQX (30 μM) and D-AP5 (50 μM), and picrotoxin (100 μM), which blocks $GABA_A$ receptors. *B*, mean number of APs before and after glutamatergic afferent stimulation ($n = 5$) in normal aCSF and in aCSF containing MPEP (50 μM; $n = 4$) or TTX (20 nM; $n = 6$). *C*, representative ADPs induced by glutamatergic afferent stimulation in the absence and in the presence of the non-selective glutamate transporter blocker TBOA (100 μM). *D*, bar graph showing the mean ADP amplitudes under conditions described in *C*.

Discussion

Expression of mGluR5 in the NAc has been demonstrated by immunohistochemistry (Shigemoto *et al.* 1993), mRNA *in situ* hybridization (Testa *et al.* 1994), and electron microscopy (Mitrano & Smith, 2007). The mechanisms underlying mGluR5 signalling in this brain area are of high interest given these receptors' involvement in self-administration of cocaine and the locomotor effects of this drug (Chiamulera *et al.* 2001). The functional relevance of mGluR5 signalling in brain structures involved in addiction is also stressed by a recent report showing that mGluR5-mediated slow afterpotential underlies persistent firing increase in the prefrontal cortex (Sidiropoulou *et al.* 2009). These authors proposed that the effects they observed represent a form of short-term cellular memory that is modulated by dopamine and cocaine experience.

Here we describe a cellular mechanism dependent on mGluR5 activation which has a strong impact on the excitability of MSNs by enhancing AP firing and, consequently, influencing the ability of these neurons to process information. In particular, we provide novel evidence that mGluR5 activation in MSNs produces I_{NaP} increases that lead to ADP.

Several mechanisms could contribute to the mGluR-dependent increases in excitability, but modulation of spike afterpotentials (AHP and ADP) is one of the strongest candidates. DHPG is known to increase the excitability of CA1 pyramidal neurons by suppressing slow and medium-duration AHPs. This effect is mediated by mGluR5 and mGluR1 via mechanisms that are PLC, PKC, and IP_3 independent (Ireland & Abraham, 2002). Persistent reduction of AHP by DHPG has been also described in layer V pyramidal neurons in the rat sensorimotor cortex (Sourdet *et al.* 2003) and in CA3 hippocampal pyramidal neurons (Young *et al.* 2004). In our experimental model, the stimulation protocol used to elicit afterpotentials never evoked AHP, and this finding is consistent with the absence of AHP in MSNs reported by other groups (Kawaguchi *et al.* 1989; Ade *et al.* 2008). We found instead that DHPG triggers ADP in MSNs of the NAc. This phenomenon was rarely observed under basal conditions and, when present, its amplitude was very small, but during exposure to DHPG '*de novo*' ADP was observed in almost all the tested cells.

ADPs have been described in many central and peripheral neurons (Connors *et al.* 1982; Li & Hatton, 1997; Staff *et al.* 2000). Although ADP has been recorded under basal conditions, it can also appear *de novo* following stimulation of numerous G-protein-coupled receptors, including muscarinic acetylcholine, α_1-noradrenergic, 5-HT_2, dopamine D1, and metabotropic glutamate receptors (Constanti *et al.* 1993; Greene *et al.* 1994; Haj-Dahmane & Andrade, 1999; McQuiston & Madison, 1999; Young *et al.* 2004; Zhang & Arsenault, 2005; Yamamoto *et al.* 2007).

Pharmacological dissection of DHPG's effects in our experimental model revealed that ADP depends on mGluR5 activation and that the pathway primarily responsible for its development is G-protein/PLC/Ca^{2+} dependent.

In different experimental models ADP has been attributed to low- and high-voltage-activated calcium currents (Li & Hatton, 1997; Metz *et al.* 2005), hyperpolarization-activated currents (Lüthi *et al.* 1998), calcium-activated non-selective cation currents (Greene *et al.* 1994), and outward potassium currents (Li & Hatton, 1997; Yue & Yaari, 2004). Our data indicate that Na^+ currents are the major driver of ADP development in NAc MSNs. The inward afterspike currents elicited by voltage commands decreased markedly during TTX exposure, which also prevented ADP in current-clamp recordings. ADP was also unaffected by Cd^{2+} and low extracellular Ca^{2+} levels, thus excluding the involvement of voltage-gated calcium channels and calcium-activated potassium channels.

Here we provide novel evidence on I_{NaP}-dependent ADP triggered by mGluR5 activation. This conclusion is based on the following observations: (1) I_{NaP} amplitude is increased by DHPG, and this effect was never observed in the presence of MPEP; (2) ADP amplitude is reduced in the presence of the selective I_{NaP} blockers riluzole and TTX (20 nM). These observations are in agreement with previous studies showing the involvement of I_{NaP} in mediating spontaneous ADP in the absence of neurotransmitter receptor activation (Yue *et al.* 2005; Chu & Moenter, 2006).

Ours is the first attempt to characterize I_{NaP} in NAc MSNs. This current seems to have the biophysical and pharmacological properties attributed to I_{NaP} in other mammalian neurons, including: (1) an activation threshold between −55 and −60 mV and a peak between −20 and −30 mV; and (2) sensitivity to both TTX and riluzole (Del Negro *et al.* 2002; Taddese & Bean, 2002; Koizumi & Smith, 2008). In addition, our study provides novel evidence that this current is modulated by mGluR5 activation. To our knowledge, glutamate-mediated modulation of I_{NaP} has previously been reported only in rat neocortical pyramidal neurons but in this model it was related to mGluR1 activation (Carlier *et al.* 2006). In this study the authors reported a mGluR1-dependent decrease of transient Na^+ current (I_{NaT}) associated with a leftward shift of the current-to-voltage relationship of I_{NaP}. However these authors suggested that the combination of the two effects of mGluR1 activation on Na^+ currents resulted in a decreased neuronal excitability.

The involvement of I_{NaP} might explain why ADP does not occur under basal conditions. The membrane

potentials associated with the initiation and development of I_{NaP} in the absence of DHPG (from −50 to 0 mV) fall within the range of potentials at which outward potassium currents mediating repolarization prevail. In contrast, in the presence of DHPG, I_{NaP} appears at membrane potentials of ∼ −60 mV, and at this level, it might result in a significant inward aftercurrent that generates ADP. Moreover, I_{NaP} have been recorded in the presence of 0.2 mM Cd^{2+}, which blocks voltage-gated Ca^{2+} channels and shifts the Na^+ current-to-voltage relationship toward more hyperpolarized potentials (Hille *et al.* 1975; Yue *et al.* 2005). It is thus conceivable that in Cd^{2+}-free aCSF, the amplitude of I_{NaP} within the voltage range associated with spike ADP development is large enough to prevail over hyperpolarizing outward potassium currents and produce a net depolarization.

In several neuronal types, I_{NaP} is involved in the control of membrane excitability within the voltage range just below the threshold for spike production (Boehmer *et al.* 2000). In tuberomammillary, subthalamic, and suprachiasmatic nucleus neurons, subthreshold Na^+ currents drive spontaneous spike discharge (Pennartz *et al.* 1997; Taddese & Bean, 2002; Do & Bean, 2004).

Here we show that the increased MSN excitability caused by mGluR5 activation is markedly attenuated by 20 nM TTX, which selectively affects I_{NaP}. We suggest, therefore, that mGluR5 activation upregulates I_{NaP}, thereby inducing an ADP that results in enhanced MSN excitability. Interestingly, stimulation of glutamatergic afferents to the NAc under ionotropic receptor blockade led to a I_{NaP}-dependent increased spike firing and appearance of ADP suggesting that the mechanism we documented operates under physiological conditions. ADP amplitude following glutamatergic afferent stimulation was smaller than that induced by DHPG whereas the increases in MSN spike firing elicited by afferent stimulation were similar to those produced pharmacologically. While it is not surprising that the pharmacological activation of mGluR5 produces effects greater than those of the receptor synaptic activation, the reason why either ADP requires larger amounts of neurotransmitter to reach its maximum or smaller ADPs are sufficient to produce maximum firing increases remains to be elucidated.

Our study also shows that mGluR5 activation in MSNs causes membrane depolarization likely to be through stimulation of Na^+/Ca^{2+} exchanger activity. Although this effect certainly contributes to increase MSN excitability, it is not primarily responsible for the enhanced spike firing and ADP we reported because these effects were recorded after injection of hyperpolarized currents compensating for membrane potential changes induced by the Na^+/Ca^{2+} exchanger activation. Moreover, ADP was unaffected by the blockade of Na^+/Ca^{2+} exchanger.

As for the functional impact of mGluR5 activation on NAc MNS excitability *in vivo*, it is important to recall that excitatory synaptic inputs to the dendritic regions of these cells trigger transitions between hyperpolarized down-states and depolarized up-states associated with spiking (Wilson & Kawaguchi, 1996; Goto & O'Donnell, 2001). By increasing the amplitude of I_{NaP} and shifting its activation threshold to a more hyperpolarized voltage range, mGluR5 activation would increase subthreshold currents in the up-state potentials and thereby enhance spike firing. In addition the mGluR5-dependent enhancement of Na^+/Ca^{2+} exchanger activity and the consequent membrane depolarization affect the resting membrane potential, which is the foundation upon which up- and down-states originate. In this way, mGluR5 activation could increase the output signals of up-state MSNs in response to synchronized excitatory inputs.

With regard to the potential implications of our findings within the context of drug-induced behaviours, it is noteworthy that changes in glutamate neurotransmission within the NAc play a significant role in neuroadaptive responses to acute or chronic cocaine exposure (Robinson & Berridge, 2003). *In vivo* microdialysis experiments have documented marked increases of extracellular glutamate levels in the NAc after acute cocaine administration (Smith *et al.* 1995; Reid *et al.* 1997). These increases have been attributed to enhanced synaptic release of neurotransmitters from prefrontal cortex afferents (McFarland *et al.* 2003). The mGluR5-dependent enhancement of MSN excitability we observed could conceivably represent one of the mechanisms by which elevated extracellular glutamate levels following acute cocaine use induce drug-seeking behaviour. Moreover, in mice treated with cocaine for 1 week, extracellular glutamate levels are significantly reduced 3 weeks after drug withdrawal (Pierce *et al.* 1996; Baker *et al.* 2003), suggesting that diminished activation of mGluR5 could contribute to cocaine relapse.

Collectively, our results provide novel evidence of important mGluR5 functions in MSNs of the NAc, which are fundamental for defining the mechanisms underlying mGluR5-dependent drug-induced behaviours.

References

Ade KK, Janssen MJ, Ortinski PI & Vicini S (2008). Differential tonic GABA conductances in striatal medium spiny neurons. *J Neurosci* **28**, 1185–1197.

Annunziato L, Pignataro G & Di Renzo GF (2004). Pharmacology of brain Na^+/Ca^{2+} exchanger: from molecular biology to therapeutic perspectives. *Pharmacol Rev* **56**, 633–654.

Aoki T, Narita M, Shibasaki M & Suzuki T (2004). Metabotropic glutamate receptor 5 localized in the limbic forebrain is critical for the development of morphine-induced rewarding effect in mice. *Eur J Neurosci* **20**, 1633–1638.

Baker DA, McFarland K, Lake RW, Shen H, Tang XC, Toda S & Kalivas PW (2003). Neuroadaptations in cystine-glutamate exchange underlie cocaine relapse. *Nat Neurosci* **6**, 743–749.

Bean BP (2007). The action potential in mammalian central neurons. *Nat Rev Neurosci* **8**, 451–465.

Beck H & Yaari Y (2008). Plasticity of intrinsic neuronal properties in CNS disorders. *Nat Rev Neurosci* **9**, 357–369.

Bkaily G, Jaalouk D, Sader S, Shbaklo H, Pothier P, Jacques D, D'Orléans-Juste P, Cragoe EJ Jr & Bose R (1998). Taurine indirectly increases $[Ca]_i$ by inducing Ca^{2+} influx through the Na^+-Ca^{2+} exchanger. *Mol Cell Biochem* **188**, 187–197.

Boehmer G, Greffrath W, Martin E & Hermann S (2000). Subthreshold oscillation of the membrane potential in magnocellular neurones of the rat supraoptic nucleus. *J Physiol* **1**, 115–128.

Carlier E, Sourdet V, Boudkkazi S, Déglise P, Ankri N, Fronzaroli-Molinieres L & Debanne D (2006). Metabotropic glutamate receptor subtype 1 regulates sodium currents in rat neocortical pyramidal neurons. *J Physiol* **577**, 141–154.

Chiamulera C, Epping-Jordan MP, Zocchi A, Marcon C, Cottiny C, Tacconi S, Corsi M, Orzi F & Conquet F (2001). Reinforcing and locomotor stimulant effects of cocaine are absent in mGluR5 null mutant mice. *Nat Neurosci* **4**, 873–874.

Chu Z & Moenter SM (2006). Physiologic regulation of a tetrodotoxin-sensitive sodium influx that mediates a slow afterdepolarization potential in gonadotropin-releasing hormone neurons: possible implications for the central regulation of fertility. *J Neurosci* **26**, 11961–11973.

Connors BW, Gutnick MJ & Prince DA (1982). Electrophysiological properties of neocortical neurons in vitro. *J Neurophysiol* **48**, 1302–1320.

Constanti A, Bagetta G & Libri V (1993). Persistent muscarinic excitation in guinea-pig olfactory cortex neurons: involvement of a slow post-stimulus afterdepolarizing current. *Neuroscience* **56**, 887–904.

D'Ascenzo M, Fellin T, Terunuma M, Revilla-Sanchez R, Meaney DF, Auberson YP, Moss SJ & Haydon PG (2007). mGluR5 stimulates gliotransmission in the nucleus accumbens. *Proc Natl Acad Sci U S A* **104**, 1995–2000.

Del Negro CA, Koshiya N, Butera RJ & Smith JC (2002). Persistent sodium current, membrane properties and bursting behaviour of pre-Bötzinger complex inspiratory neurons in vitro. *J Neurophysiol* **88**, 2242–2250.

Do MT & Bean BP (2004). Sodium currents in subthalamic nucleus neurons from Nav1.6-null mice. *J Neurophysiol* **92**, 726–733.

Dong Y, Green T, Saal D, Marie H, Neve R, Nestler EJ & Malenka RC (2006). CREB modulates excitability of nucleus accumbens neurons. *Nat Neurosci* **9**, 475–477.

Everitt BJ & Wolf ME (2002). Psychomotor stimulant addiction: a neural systems perspective. *J Neurosci* **22**, 3312–3320.

Fellin T, Pozzan T & Carmignoto G (2006). Purinergic receptors mediate two distinct glutamate release pathways in hippocampal astrocytes. *J Biol Chem* **281**, 4274–4284.

French CR, Sah P, Buckett KJ & Gage PW (1990). A voltage-dependent persistent sodium current in mammalian hippocampal neurons. *J Gen Physiol* **95**, 1139–1157.

Galarraga E, Pacheco-Cano MT, Flores-Hernández JV & Bargas J (1994). Subthreshold rectification in neostriatal spiny projection neurons. *Exp Brain Res* **100**, 239–249.

Goto Y & Grace AA (2008). Limbic and cortical information processing in the nucleus accumbens. *Trends Neurosci* **31**, 552–558.

Goto Y & O'Donnell P (2001). Network synchrony in the nucleus accumbens in vivo. *J Neurosci* **21**, 4498–4504.

Greene CC, Schwindt PC & Crill WE (1994). Properties and ionic mechanisms of a metabotropic glutamate receptor-mediated slow afterdepolarization in neocortical neurons. *J Neurophysiol* **72**, 693–704.

Groenewegen HJ, Becker NE & Lohman AH (1980). Subcortical afferents of the nucleus accumbens septi in the cat, studied with retrograde axonal transport of horseradish peroxidase and bisbenzimid. *Neuroscience* **5**, 1903–1916.

Grunnet M, Jespersen T, Angelo K, Frøkjaer-Jensen C, Klaerke DA, Olesen SP & Jensen BS (2001). Pharmacological modulation of SK3 channels. *Neuropharmacology* **40**, 879–887.

Haj-Dahmane S & Andrade R (1999). Muscarinic receptors regulate two different calcium-dependent non-selective cation currents in rat prefrontal cortex. *Eur J Neurosci* **11**, 1973–1980.

Hille B, Woodhull AM & Shapiro BI (1975). Negative surface charge near sodium channels of nerve: divalent ions, monovalent ions, and pH. *Philos Trans R Soc Lond B Biol Sci* **270**, 301–318.

Hopf FW, Cascini MG, Gordon AS, Diamond I & Bonci A (2003). Cooperative activation of dopamine D1 and D2 receptors increases spike firing of nucleus accumbens neurons via G-protein $\beta\gamma$ subunits. *J Neurosci* **23**, 5079–5087.

Horowitz LF, Hirdes W, Suh BC, Hilgemann DW, Mackie K & Hille B (2005). Phospholipase C in living cells: activation, inhibition, Ca^{2+} requirement, and regulation of M current. *J Gen Physiol* **126**, 243–262.

Huang H & Van Den Pol AN (2007). Rapid direct excitation and long-lasting enhancement of NMDA response by group I metabotropic glutamate receptor activation of hypothalamic melanin-concentrating hormone neurons. *J Neurosci* **27**, 11560–11572.

Ireland DR & Abraham WC (2002). Group I mGluRs increase excitability of hippocampal CA1 pyramidal neurons by a PLC-independent mechanism. *J Neurophysiol* **88**, 107–116.

Jeffs GJ, Meloni BP, Bakker AJ & Knuckey NW (2007). The role of the Na^+/Ca^{2+} exchanger (NCX) in neurons following ischaemia. *J Clin Neurosci* **14**, 507–514.

Kauer JA & Malenka RC (2007). Synaptic plasticity and addiction. *Nat Rev Neurosci* **8**, 844–858.

Kawaguchi Y, Wilson CJ & Emson PC (1989). Intracellular recording of identified neostriatal patch and matrix spiny cells in a slice preparation preserving cortical inputs. *J Neurophysiol* **62**, 1052–1068.

Koizumi H & Smith JC (2008). Persistent Na^+ and K^+-dominated leak currents contribute to respiratory rhythm generation in the pre-Bötzinger complex in vitro. *J Neurosci* **28**, 1773–1785.

LaLumiere RT & Kalivas PW (2008). Glutamate release in the nucleus accumbens core is necessary for heroin seeking. *J Neurosci* **28**, 3170–3177.

Largo C, Cuevas P, Somjen GG, Martin del Rio R & Herreras O (1996). The effect of depressing glial function in rat brain in situ on ion homeostasis, synaptic transmission, and neuron survival. *J Neurosci* **16**, 1219–1229.

Li Z & Hatton GI (1997). Reduced outward K^+ conductances generate depolarizing after-potentials in rat supraoptic nucleus neurones. *J Physiol* **505**, 95–106.

Lüthi A, Bal T & McCormick DA (1998). Periodicity of thalamic spindle waves is abolished by ZD7288, a blocker of I_h. *J Neurophysiol* **79**, 3284–3289.

Martín ED, Fernández M, Perea G, Pascual O, Haydon PG, Araque A & Ceña V (2007). Adenosine released by astrocytes contributes to hypoxia-induced modulation of synaptic transmission. *Glia* **55**, 36–45.

McFarland K, Lapish CC & Kalivas PW (2003). Prefrontal glutamate release into the core of the nucleus accumbens mediates cocaine-induced reinstatement of drug-seeking behaviour. *J Neurosci* **23**, 3531–3537.

McQuiston AR & Madison DV (1999). Muscarinic receptor activity induces an afterdepolarization in a subpopulation of hippocampal CA1 interneurons. *J Neurosci* **19**, 5703–5710.

Metz AE, Jarsky T, Martina M & Spruston N (2005). R-type calcium channels contribute to afterdepolarization and bursting in hippocampal CA1 pyramidal neurons. *J Neurosci* **25**, 5763–5773.

Mitrano DA & Smith Y (2007). Comparative analysis of the subcellular and subsynaptic localization of mGluR1a and mGluR5 metabotropic glutamate receptors in the shell and core of the nucleus accumbens in rat and monkey. *J Comp Neurol* **500**, 788–806.

Nestler EJ (2001). Molecular neurobiology of addiction. *Am J Addict* **10**, 201–217.

Pace RW, Mackay DD, Feldman JL & Del Negro CA (2007). Role of persistent sodium current in mouse preBötzinger complex neurons and respiratory rhythm generation. *J Physiol* **580**, 485–496.

Pennartz CM, Bierlaagh MA & Geurtsen AM (1997). Cellular mechanisms underlying spontaneous firing in rat suprachiasmatic nucleus: involvement of a slowly inactivating component of sodium current. *J Neurophysiol* **78**, 1811–1825.

Pierce RC, Bell K, Duffy P & Kalivas PW (1996). Repeated cocaine augments excitatory amino acid transmission in the nucleus accumbens only in rats having developed behavioural sensitization. *J Neurosci* **16**, 1550–1560.

Pin JP & Duvoisin R (1995). The metabotropic glutamate receptors: structure and functions. *Neuropharmacology* **34**, 1–26.

Plenz D & Kitai ST (1998). Up and down states in striatal medium spiny neurons simultaneously recorded with spontaneous activity in fast-spiking interneurons studied in cortex-striatum-substantia nigra organotypic cultures. *J Neurosci* **18**, 266–283.

Popik P & Wróbel M (2002). Morphine conditioned reward is inhibited by MPEP, the mGluR5 antagonist. *Neuropharmacology* **43**, 1210–1217.

Reid MS, Hsu K Jr & Berger SP (1997). Cocaine and amphetamine preferentially stimulate glutamate release in the limbic system: studies on the involvement of dopamine. *Synapse* **27**, 95–105.

Robbe D, Kopf M, Remaury A, Bockaert J & Manzoni OJ (2002). Endogenous cannabinoids mediate long-term synaptic depression in the nucleus accumbens. *Proc Natl Acad Sci U S A* **99**, 8384–8388.

Robinson TE & Berridge KC (2003). Addiction. *Annu Rev Psychol* **54**, 25–53.

Sekizawa S & Bonham AC (2006). Group I metabotropic glutamate receptors on second-order baroreceptor neurons are tonically activated and induce a Na^+-Ca^{2+} exchange current. *J Neurophysiol* **95**, 882–892.

Shen W, Hernandez-Lopes S, Tkatch T, Held JE & Surmeier DJ (2004). $K_V1.2$-containing K^+ channels regulate subthreshold excitability of striatal medium spiny neurons. *J Neurophysiol* **91**, 1337–1349.

Shigemoto R, Nomura S, Ohishi H, Sugihara H, Nakanishi S & Mizuno N (1993). Immunohistochemical localization of a metabotropic glutamate receptor, mGluR5, in the rat brain. *Neurosci Lett* **163**, 53–57.

Sidiropoulou K, Lu FM, Fowler MA, Xiao R, Phillips C, Ozkan ED, Zhu MX, White FJ & Cooper DC (2009). Dopamine modulates an mGluR5-mediated depolarization underlying prefrontal persistent activity. *Nat Neurosci* **12**, 190–199.

Smith JA, Mo Q, Guo H, Kunko PM & Robinson SE (1995). Cocaine increases extraneuronal levels of aspartate and glutamate in the nucleus accumbens. *Brain Res* **683**, 264–269.

Sourdet V, Russier M, Daoudal G, Ankri N & Debanne D (2003). Long-term enhancement of neuronal excitability and temporal fidelity mediated by metabotropic glutamate receptor subtype 5. *J Neurosci* **23**, 10238–10248.

Staff NP, Jung HY, Thiagarajan T, Yao M & Spruston N (2000). Resting and active properties of pyramidal neurons in subiculum and CA1 of rat hippocampus. *J Neurophysiol* **84**, 2398–2408.

Taddese A & Bean BP (2002). Subthreshold sodium current from rapidly inactivating sodium channels drives spontaneous firing of tuberomammillary neurons. *Neuron* **33**, 587–600.

Tessari M, Pilla M, Andreoli M, Hutcheson DM & Heidbreder CA (2004). Antagonism at metabotropic glutamate 5 receptors inhibits nicotine- and cocaine-taking behaviours and prevents nicotine-triggered relapse to nicotine-seeking. *Eur J Pharmacol* **499**, 121–133.

Testa CM, Standaert DG, Young AB & Penney JB (1994). Metabotropic glutamate receptor mRNA expression in the basal ganglia of the rat. *J Neurosci* **14**, 3005–3018.

Thomas MJ, Beurrier C, Bonci A & Malenka RC (2001). Long-term depression in the nucleus accumbens: a neural correlate of behavioural sensitization to cocaine. *Nat Neurosci* **4**, 1217–1223.

Tortiglione A, Picconi B, Barone I, Centonze D, Rossi S, Costa C, Di Filippo M, Tozzi A, Tantucci M, Bernardi G, Annunziato L & Calabresi P (2007). Na^+/Ca^{2+} exchanger maintains ionic homeostasis in the peri-infarct area. *Stroke* **38**, 1614–1620.

Wilson CJ & Kawaguchi Y (1996). The origins of two-state spontaneous membrane potential fluctuations of neostriatal spiny neurons. *J Neurosci* **16**, 2397–2410.

Wu SN & Li HF (1999). Characterization of riluzole-induced stimulation of large-conductance calcium-activated potassium channels in rat pituitary GH3 cells. *J Investig Med* **47**, 484–95.

Yamamoto R, Ueta Y & Kato N (2007). Dopamine induces a slow afterdepolarization in lateral amygdala neurons. *J Neurophysiol* **98**, 984–992.

Young SR, Chuang SC & Wong RK (2004). Modulation of afterpotentials and firing pattern in guinea pig CA3 neurones by group I metabotropic glutamate receptors. *J Physiol* **554**, 371–385.

Yue C & Yaari Y (2004). KCNQ/M channels control spike afterdepolarization and burst generation in hippocampal neurons. *J Neurosci* **24**, 4614–4624.

Yue C, Remy S, Su H, Beck H & Yaari Y (2005). Proximal persistent Na^+ channels drive spike afterdepolarizations and associated bursting in adult CA1 pyramidal cells. *J Neurosci* **25**, 9704–9720.

Zhang ZW & Arsenault D (2005). Gain modulation by serotonin in pyramidal neurones of the rat prefrontal cortex. *J Physiol* **566**, 379–394.

Author contributions

M.D'A. contributed to the conception and design of experiments, performed the experiments, analysed the data, contributed to their interpretation and drafted the article. M.V.P. contributed to design and conduct some experiments, contributed to data interpretation and drafted the manuscript. T.F. contributed to data interpretation and to revising the manuscript. P.H., C.G. and G.B.A. contributed to the conception and design of the study, critically reviewed the manuscript for important intellectual content and contributed to data interpretation. All authors gave the final approval of the version to be published. The experiments were performed at the Catholic University School of Medicine in Rome, Italy.

Acknowledgments

We are grateful to Prof. Lucio Annunziato (School of Medicine, Federico II University of Naples) for generously providing CB-DMB and to Dr. Elisa Riccardi for assistance in brain slice preparations. This work was supported by grants from Catholic University (D1 funds) to C.G.